Ferromagnetic Resonance of a Single Magnetochiral Metamolecule of Permalloy

Toshiyuki Kodama,[1] Satoshi Tomita,[1,*] Takeshi Kato,[2] Daiki Oshima,[3] Satoshi Iwata,[3] Satoshi Okamoto,[4] Nobuaki Kikuchi,[4] Osamu Kitakami,[4] Nobuyoshi Hosoito,[1] and Hisao Yanagi[1]

[1]*Graduate School of Materials Science, Nara Institute of Science and Technology, Ikoma, Nara 630-0192, Japan*

[2]*Graduate School of Engineering, Nagoya University, Chikusa, Nagoya 464-8603, Japan*

[3]*Institute of Materials and Systems for Sustainability, Nagoya University, Chikusa, Nagoya 464-8603, Japan*

[4]*Institute of Multidisciplinary Research for Advanced Materials, Tohoku University, Katahira, Sendai 980-8577, Japan*

(Received 16 October 2015; revised manuscript received 28 April 2016; published 24 August 2016)

We investigate the ferromagnetic resonance (FMR) of a single chiral structure of a ferromagnetic metal—the magnetochiral (MCh) metamolecule. Using a strain-driven self-coiling technique, micrometer-sized MCh metamolecules of metallic permalloy (Py) are fabricated without any residual Py films. The magnetization curves of ten Py MCh metamolecules obtained by an alternating gradient magnetometer show soft magnetic behavior. In cavity FMR with a magnetic-field sweep and coplanar-waveguide (CPW) FMR with a frequency sweep, the Kittel-mode FMR of the single Py metamolecule is observed. The CPW-FMR results, which are consistent with the cavity-FMR results, bring about the effective g factor, effective magnetization, and Gilbert damping of the single metamolecule. Together with calculations using these parameters, the angle-resolved cavity FMR reveals that the magnetization in the Py MCh metamolecule is most likely to be the hollow-bar type of configuration when the external magnetic field is applied parallel to the chiral axis, although the expected magnetization state at remanence is the corkscrew type of configuration.

DOI: 10.1103/PhysRevApplied.6.024016

I. INTRODUCTION

Symmetry breaking in condensed matter brings about intriguing electromagnetic properties [1]. The break in the space-inversion symmetry in chiral structures causes optical activity, while the break in the time-reversal symmetry in magnetized materials leads to magneto-optical effects. In particular, simultaneous space-inversion and time-reversal symmetry breaking gives rise to a directional birefringence independent of polarizations [2–6]. Directional birefringence is a key phenomenon in the realization of a "one-way mirror" [7] and an artificial gauge field for electromagnetic waves [8,9]. The system with both space-inversion and time-reversal symmetries broken is of interest also in terms of topological spin textures like the Skyrmion [10,11]. It is, however, a challenge to break the symmetries simultaneously in natural materials without a high magnetic field or low temperature. Therefore, artificial materials consisting of microstructures much smaller than the electromagnetic-wave wavelength—metamaterials [12]—are a way to mimic natural materials with magnetism and chirality at a modest magnetic field and room temperature.

Metamaterials are composed of metamolecules, which are the smallest unit cells exhibiting intriguing electromagnetic responses. It has been reported very recently that millimeter-sized metamolecules with magnetism and chirality—magnetochiral (MCh) metamolecules—demonstrate directional birefringence for the X-band microwaves at room temperature [13]. Since the operational frequency scales the metamolecules with size, miniaturization is required for the directional-birefringence realization at higher frequencies, for example, millimeter waves and terahertz waves. Nevertheless, owing to their three-dimensional (3D) structures, micrometer-sized MCh metamolecules are difficult to prepare using only standard microprocessing with photolithography and etching.

Strain-driven self-coiling is a powerful technique for preparing three-dimensional structures of metallic thin films [14–20]. In previous work [21], we fabricated micrometer-sized chiral structures of ferromagnetic metallic cobalt (Co) films, like magnetic microhelix coils, using a strain-driven self-coiling technique with two-step photolithography followed by lift-off processes [22]. An array of dozens of the Co MCh metamolecules are fixed and aligned in the same direction on a substrate. The angle-resolved ferromagnetic resonance (FMR) of the metamolecule array in a cavity is studied for the elucidation of the magnetization configuration in the metamolecules by varying the external dc-magnetic-field direction. When the dc magnetic field is applied parallel to the chiral axis, a hollow-bar-type magnetization configuration [17] in the chiral structures is essential for obtaining directional birefringence.

*tomita@ms.naist.jp

While the Co MCh metamolecule array shows FMR signals in the previous study, the detailed behavior and true origin of the signals are under debate owing to inhomogeneous broadening caused by metamolecule-orientation randomness. The inhomogeneous broadening is also caused by additional resonances attributed to residual Co films on the substrate due to the two-step lithography and lift-off processes. As a result, the magnetization configuration has yet to be elucidated for metamolecules. Furthermore, the dynamical magnetic properties, for example, the g value and Gilbert damping factor, of the metamolecules are unclear.

In this work, we succeed in studying the FMR by a single MCh metamolecule of permalloy ($Fe_{21.5}Ni_{78.5}$) (Py) without any residual Py films. Micrometer-sized and freestanding Py MCh metamolecules fabricated using the strain-driven self-coiling technique are transferred to another substrate for magnetization and FMR measurements. A small magnetization of ten Py MCh metamolecules is measured. Angle-resolved FMR studies are conducted for a single metamolecule in a cavity, which is taken from the ten metamolecules after the magnetization measurements. The single metamolecule highlights two types of Kittel-mode FMR: One shifts slightly to a lower field of 100 mT, and the other shifts significantly to a higher field as the magnetic field is applied perpendicular to the chiral axis. The Kittel mode that shifts significantly to a higher field is accompanied by the localized resonance mode. Frequency-sweep FMR of another single Py MCh metamolecule on a coplanar waveguide (CPW) confirms the Kittel-mode FMR; the effective g factor, effective magnetization, Gilbert damping, and extrinsic broadening factor are experimentally evaluated. These FMR studies together with a theoretical calculation reveal that the magnetization in the metamolecule is aligned in the dc-magnetic-field direction (i.e., the hollow-bar-type configuration) when the magnetic field is applied parallel to the chiral axis, even though the expected magnetization state at remanence is azimuthal or helical (i.e., the corkscrew-type configuration). The hollow-bar-type configuration under the magnetic field is essential for obtaining a directional birefringence using the MCh metamolecule.

II. EXPERIMENTAL RESULTS

A. Sample preparation and magnetization measurements

SU8 3005 photoresist (Nippon Kayaku) 5 μm in thickness is spin-coated on a Si substrate. Inverse S-shaped strips are patterned on the resist using photolithography [Fig. 1(a)]. The strip length is 1.1 mm, and the strip width is 9 μm. Py is deposited on the sample using a magnetron sputtering technique with an argon gas pressure of 4.2×10^{-3} Torr [Fig. 1(b)]. The Py deposition rate is 0.1 nm/s as calibrated by an x-ray reflectometer. The Py layer thickness is 60 nm.

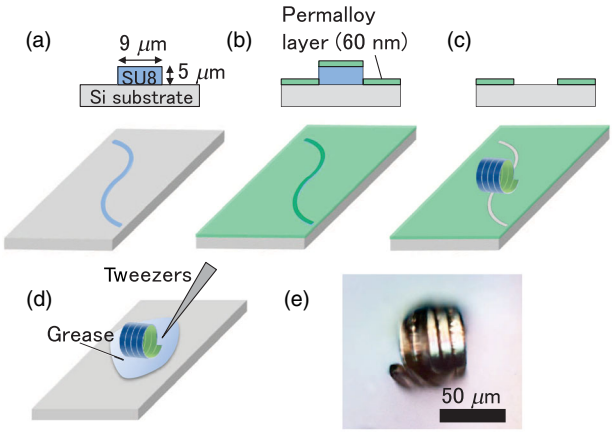

FIG. 1. (a)–(d) Fabrication procedures of Py MCh metamolecule using the strain-driven self-coiling technique. (e) Optical-microscopic image of a single metamolecule fixed by grease on a silicon substrate.

By dipping the sample into *N*-methyl-2-pyrrolidone, the strips coil spontaneously, resulting in the formation of freestanding Py MCh metamolecules [Fig. 1(c)]. The freestanding metamolecules are transferred to another Si substrate using tweezers and fixed by grease [Fig. 1(d)]. After the transfer process, the metamolecule modification in shape and ellipticity is not observed.

In the present preparation processes, we do not use two-step lithography followed by lift-off processes. Such improvements enable us to realize the Py MCh metamolecule sample without any residual Py films on the substrates. Figure 1(e) shows an optical-microscope image of the metamolecule fixed by grease on the Si substrate after a transfer. As in Fig. 1(e), the strip coils up six times, and the metamolecule length and diameter are about 50 μm. The coiling direction is clockwise, indicating that the strip coils up toward the outside of the curvature as we previously reported [21]. We succeed in controlling the coiling direction using S-shaped or inverse S-shaped strips. Additionally, because the Py thin films are supported by the rigid SU8 resist strips about 5 μm in thickness, a procedure to preserve the microstructures (e.g., critical point drying) is unnecessary.

The Py volume in the single metamolecule is calculated at approximately 6.1×10^{-16} m^3. Since this volume is very small, even ten Py metamolecules give rise to a small magnetic moment, which is difficult to measure using a standard magnetometer (e.g., vibrating sample magnetometer). Therefore, we use an alternating gradient magnetometer (AGM; Lake Shore PMC MicroMag 2900) for the magnetization measurement of the ten Py metamolecules collected on the substrate. The metamolecule chiral axes are perpendicular to the substrate plane as illustrated in the inset in Fig. 2. The distance among metamolecules in the array is approximately 100 μm. The external dc magnetic field (H_{ext}) is applied in parallel and perpendicular to the

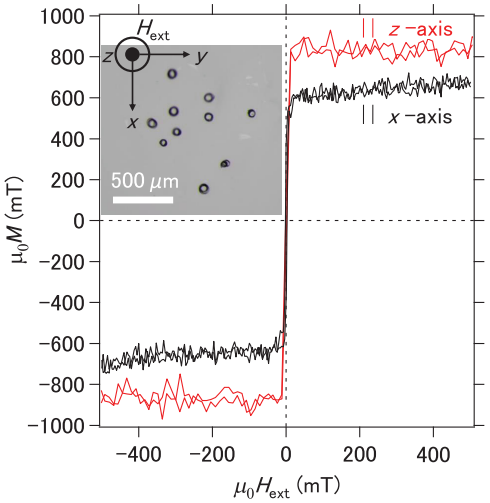

FIG. 2. Magnetization curves of ten Py metamolecules with an external dc magnetic field applied in parallel (red lines) and perpendicular (black lines) to the chiral axis.

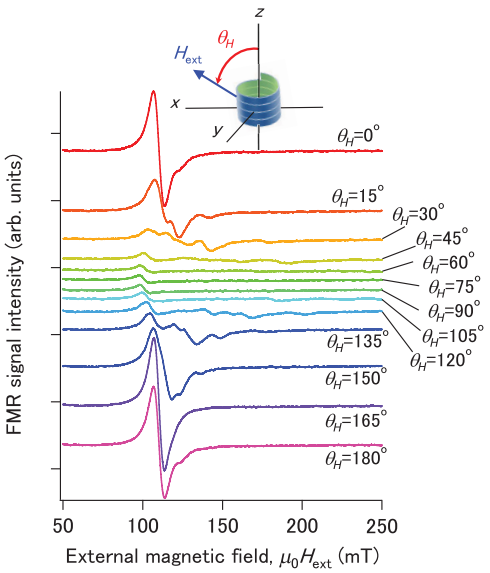

FIG. 3. Angle-resolved FMR signals of a single Py metamolecule in a cavity. The Py metamolecule for the cavity-FMR study is selected from ten metamolecules used for the magnetization measurement. The inset illustrates the definition of an external dc-magnetic-field angle.

Py metamolecules' chiral axes. The measurements are carried out at room temperature.

In Fig. 2, the magnetization ($\mu_0 M$) of the ten Py metamolecules is plotted as a function of $\mu_0 H_{ext}$. μ_0 is the magnetic permeability of the vacuum. The magnetization curve in Fig. 2 demonstrates spontaneous magnetization. The magnetization is saturated when $\mu_0 H_{ext}$ is applied parallel to the chiral axis (red curve), whereas it is not saturated with $\mu_0 H_{ext}$ applied perpendicular to the chiral axis (black curve). Saturation magnetization $\mu_0 M_s$ evaluated from the magnetization curves with parallel $\mu_0 H_{ext}$ is approximately 850 mT, which is slightly smaller than the saturation magnetization of a metallic Py thin film (1.05 T) given in the literature [23]. These results indicate that the metamolecules retain the soft magnetic nature of metallic Py.

B. Angle-resolved FMR using a cavity

After the magnetization measurements, a single Py metamolecule is picked up, transferred to another Si substrate, and fixed by grease for the angle-resolved FMR studies by varying the H_{ext} direction. The chiral axis is perpendicular to the substrate plane. Angle-resolved FMR of the single Py metamolecule in a TE_{011} cavity for the X-band microwave of 9.8 GHz is carried out using an electron spin resonance (ESR) spectrometer (JEOL JES-FA100N). H_{ext} is applied using an electromagnet. The measurements are carried out at room temperature.

Figure 3 illustrates the angle-resolved FMR spectra of the single Py metamolecule in the cavity. The inset in Fig. 3 depicts the H_{ext} configuration in the measurement. The H_{ext} angle (θ_H) is varied in the x-z plane. The angle increments are 15°. $\theta_H = 0°$ and $\theta_H = 90°$ correspond to the dc magnetic field applied parallel and perpendicular to the chiral axis, respectively. The direction of the X-band microwave ac magnetic field in the TE_{011} cavity is parallel to the y axis, in other words, perpendicular to both the metamolecule chiral axis and H_{ext}. Signal intensities are normalized using an ESR signal from manganese ions as the standard sample between 320 and 360 mT.

Figure 3 highlights two types of resonance: One shifts slightly to a lower field, and the other shifts significantly to a higher field as the angle θ_H is increased. A strong resonance at 106 mT is seen when $\theta_H = 0°$. As θ_H is increased, the resonance signal at 106 mT shifts very slightly to a lower field, and the signal intensity becomes weaker. The resonance field shifts to its lowest, about 97 mT, at $\theta_H = 75°$. The resonance moves back to a higher field accompanied by an increase in intensity when θ_H is further increased.

At $\theta_H = 15°$, additional weak resonance signals are observed at 117 and 134 mT. In contrast to the resonance at 106 mT, these resonances shift significantly to higher fields as θ_H is increased. At $\theta_H = 30°$, three weak resonance signals are observed at 114, 136, and 170 mT. These resonances disappear from the dc-magnetic-field measurement range (0–650 mT) when θ_H is between 60° and 90°. At $\theta_H = 120°$, the weak resonances are observed again at 136, 152, 161, and 190 mT. The weak resonances shift to lower fields as θ_H is increased and merge with the resonance of 106 mT at $\theta_H = 165°$.

We conduct angle-resolved cavity FMR for another ten Py metamolecules. All of the metamolecules show the weak magnetic resonances when the magnetic-field direction is oblique to the chiral axis, while a Py plain film does

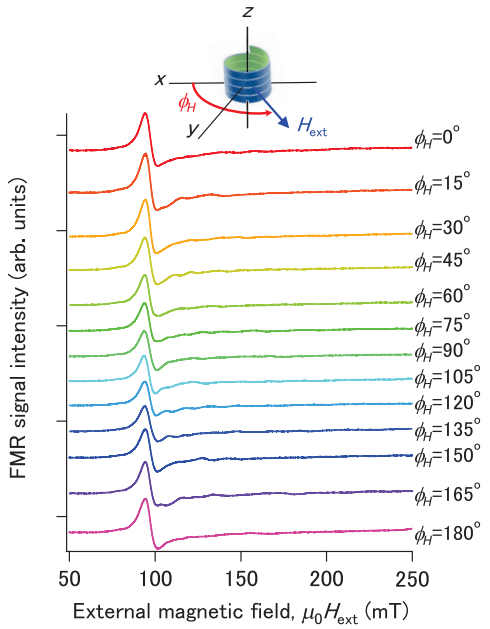

FIG. 4. FMR signals of a single Py metamolecule in a cavity when the external magnetic-field direction is changed in the *x*-*y* plane. The inset illustrates the external dc-magnetic-field orientation with respect to the chiral axis. The measured Py metamolecule is the same as that in Fig. 3.

not show the weak resonances (not shown here). The composition variation of Fe and Ni in the Py strip is unlikely in the self-coiling to the metamolecule. The weak resonances are therefore caused by the metamolecule shape, whereas the metamolecule chirality does not affect the angle-resolved FMR signals.

Figure 4 shows the cavity-FMR signals of the same Py metamolecule when the H_{ext} angle (ϕ_H) is varied in the *x*-*y* plane. H_{ext} is perpendicular to the chiral axis at any ϕ_H, as illustrated in the inset. The sample and measurement conditions are the same as those in Fig. 3. In Fig. 4, the FMR signals are identical at any ϕ_H. A resonance is seen at 94 mT, and this resonance does not shift while ϕ_H is increased. No additional resonances emerge with an increase in ϕ_H, although the spectra between 100 and 150 mT exhibit a very small ripple, of which the origin is unclear. These results prove an absence of the residual magnetic films on the substrates, whereas the metamolecule array in our previous report [21] shows a resonance signal which moves depending on ϕ_H.

C. Frequency-sweep FMR using coplanar waveguide and vector network analyzer

As illustrated in Fig. 5(a), a CPW consisting of a signal line with 82 μm in width and 1 mm in length sandwiched with two ground lines is fabricated using standard photolithography together with gold-deposition and lift-off processes. The gap between the signal and ground lines is 9 μm. A single Py metamolecule is placed at the center of the signal line as shown in Figs. 5(a) and 5(b). $\mu_0 H_{ext}$ up to 1.35 T is applied using an electromagnet. The $\mu_0 H_{ext}$ direction is parallel to the *z* axis (i.e., parallel to the chiral axis). The microwaves propagate from port 1 to port 2 in the signal line. The ac magnetic field generated by the microwave is in the *x*-axis direction, which is perpendicular to the chiral axis, $\mu_0 H_{ext}$, and the microwave propagating direction. The microwave transmission coefficients from port 1 to port 2 corresponding to the *S* parameter of S_{21} are measured using a vector network analyzer (VNA; Agilent E8363C) at room temperature. The microwave frequency is swept from 1 to 40 GHz.

Since the single metamolecule FMR signal is quite small, we derive $\Delta|S_{21}|$ as

$$\Delta|S_{21}| = |S_{21}^{raw}| - |S_{21}^{bg}|, \quad (1)$$

where S_{21}^{raw} corresponds to S_{21} under a specific nonzero magnetic field and S_{21}^{bg} to S_{21} under a zero magnetic field. S_{21}^{bg} is measured just before every measurement of S_{21}^{raw}. Figure 5(c) illustrates transmission spectra $\Delta|S_{21}|$ at various $\mu_0 H_{ext}$. When $\mu_0 H_{ext} = 100$ mT, a dip appears at approximately 8.3 GHz. The dip shifts to a higher frequency as $\mu_0 H_{ext}$ is increased. The dip finally reaches to 32.7 GHz when $\mu_0 H_{ext} = 800$ mT.

As a control, a Py strip 9 μm in width and 700 μm in length is prepared on another CPW using standard photolithography followed by the 60-nm-thickness Py deposition

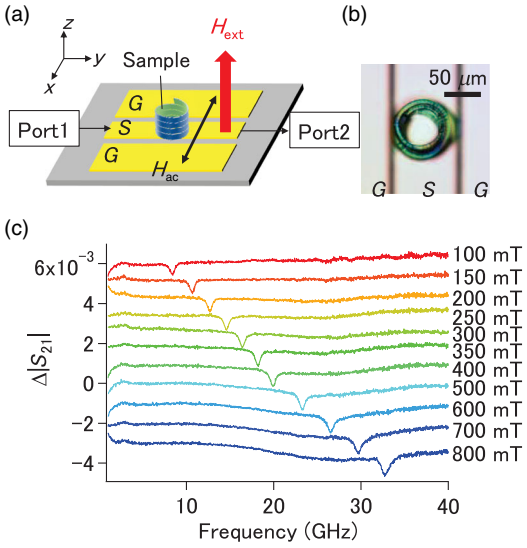

FIG. 5. (a) Schematic and (b) optical-microscope image of a single Py MCh metamolecule placed on a coplanar waveguide (*S* is the signal line, and *G* is the ground line) in the CPW-FMR measurement. The Py MCh metamolecule's chiral axis is parallel to the external dc magnetic field (H_{ext}). The ac magnetic field (H_{ac}) generated by microwaves is perpendicular to the chiral axis and H_{ext}. (c) The microwave transmission spectra of a single Py metamolecule on a CPW.

and the lift-off process. The longitudinal strip is placed at the signal line edge in CPW-FMR measurements, because the sensitivity is the highest at the edge. $\mu_0 H_{\rm ext}$ is applied in the direction parallel to the z axis. Although not shown here, a FMR signal appears at much higher $\mu_0 H_{\rm ext}$ above 1.1 T owing to the demagnetization field in the Py strip and shifts with an increase in $\mu_0 H_{\rm ext}$.

III. DISCUSSION

A. g factor, effective magnetization, and Gilbert damping of the metamolecule

The resonance frequency f_0 and full width at half maximum (FWHM) Δf of the dip in the $\Delta|S_{21}|^2$ spectra are evaluated by the fitting to the Lorentz function. Because the least-squares method is employed in the fitting, errors correspond to a standard deviation. The single Py metamolecule's f_0 are plotted as a function of $\mu_0 H_{\rm ext}$ in Fig. 6(a) (open circles). The standard deviations in f_0 are quite small, so that error bars cannot be seen in Fig. 6(a).

The most likely origin of the resonance observed in Fig. 5(c) is the Kittel-mode FMR corresponding to uniform precession of electron spins in Py films [24]. The f_0 plot in Fig. 6(a) is therefore fitted using the Kittel formula. When $\mu_0 H_{\rm ext}$ is applied in an oblique direction to the film surface with an angle of Θ_H, the Kittel formula is written as [25]

$$\left(\frac{\omega_0}{\gamma}\right)^2 = (\mu_0 H_0 + \mu_0 M_{\rm eff}\cos 2\Theta_H)(\mu_0 H_0 - \mu_0 M_{\rm eff}\sin^2\Theta_H), \tag{2}$$

where $\omega_0 = 2\pi f_0$ is the resonance angular frequency, $\gamma = g_{\rm eff}(\mu_B/\hbar)$ is the gyromagnetic ratio, $\mu_0 H_0$ is the resonance-magnetic-field strength, and $\mu_0 M_{\rm eff}$ is the effective saturation magnetization including magnetic anisotropies [26], for example, the surface and interface magnetic anisotropy. $g_{\rm eff}$ represents the effective g factor. In Eq. (2), $\Theta_H = 0°$ and 180° are assigned to $\mu_0 H_{\rm ext}$ parallel to the film plane, while $\Theta_H = 90°$ is assigned to that perpendicular to the film plane. Since $\mu_0 H_{\rm ext}$ is applied perpendicular to the CPW (i.e., parallel to the chiral axis of the metamolecule on the CPW), the present CPW-FMR measurement for the metamolecule corresponds to $\Theta_H = 0°$. Therefore, after substituting $\Theta_H = 0°$ into Eq. (2), we use the Kittel formula written as

$$\left(\frac{\omega_0}{\gamma}\right)^2 = \mu_0^2 H_0 (H_0 + M_{\rm eff}), \tag{3}$$

in the fitting.

The red solid line in Fig. 6(a) corresponds to the fitting curve by Eq. (3). The fitting procedure gives a $g_{\rm eff}$ of 2.1590 ± 0.0082 and a $\mu_0 M_{\rm eff}$ of 681.77 ± 9.01 mT. The errors represent the standard deviation in the fitting. The

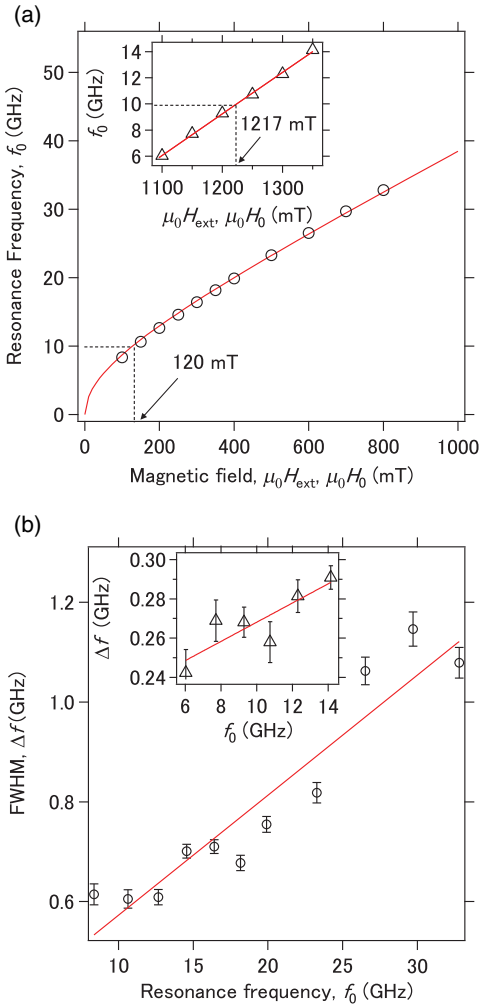

FIG. 6. (a) FMR frequencies of a Py metamolecule (open circles) and a Py strip (open triangles in the inset) measured using VNA are plotted as a function of $\mu_0 H_{\rm ext}$. The microwave frequency (9.8 GHz) used in angle-resolved FMR with a cavity and the corresponding $\mu_0 H_{\rm ext}$ for FMR are indicated by dashed lines (120 mT for the metamolecule and 1217 mT for the strip). The red solid line corresponds to a fitting curve by the Kittel formula. (b) The full width at half maximum of FMR signals of a Py metamolecule and strip (inset) is plotted as a function of the resonance frequency. The red solid line corresponds to the linear fitting line.

$\mu_0 M_{\rm eff}$ of 681.77 ± 9.01 mT evaluated from the CPW FMR is smaller than the saturation magnetization of 850 mT evaluated from the AGM magnetization curves in Fig. 2. Because $\mu_0 M_{\rm eff}$ obtained by the CPW-FMR result fitting is more appropriate for discussing dynamical magnetic properties, 681.77 ± 9.01 mT of $\mu_0 M_{\rm eff}$ is utilized in the following. The fitting curve in Fig. 6(a) indicates that a microwave frequency of 9.8 GHz used in the cavity-FMR results in the resonance field of 120 mT (dashed line). The resonance magnetic field of 120 mT is very similar to 106 mT observed in the cavity FMR at $\Theta_H = 0$ as shown in

Fig. 3. This result proves that the Kittel mode is observed in both the CPW FMR and cavity FMR.

The inset in Fig. 6(a) shows f_0 plotted as a function of $\mu_0 H_{\rm ext}$ for the Py strip fabricated on the CPW. The f_0 and Δf are obtained by fitting the dip in the $\Delta|S_{21}|^2$ spectra to the Lorentz function. Since $\mu_0 H_{\rm ext}$ is applied in the direction perpendicular to the CPW, $\Theta_H = 90°$ is substituted into Eq. (2), and the Kittel formula is obtained to be

$$\left(\frac{\omega_0}{\gamma}\right)^2 = \mu_0^2 (H_0 - M_{\rm eff})^2. \tag{4}$$

The red solid line represents the fitting curve. After the fitting, $g_{\rm eff}$ and $\mu_0 M_{\rm eff}$ are evaluated to be 2.2800 and 910.45 mT, respectively. The CPW-FMR results demonstrate that $g_{\rm eff}$ and $\mu_0 M_{\rm eff}$ decrease for the metamolecule.

Figure 6(b) illustrates a plot of Δf versus f_0 for the Py metamolecule. The inset is the corresponding plot for the Py strip as a control. The error bars in Fig. 6(b) represent standard deviations of experimentally evaluated Δf by the fitting using the Lorentz function. The effective Gilbert damping factor $\alpha_{\rm eff}$ is obtained by

$$\Delta f = 2\alpha_{\rm eff} f_0 + \Delta f^{\rm ext}, \tag{5}$$

where $\Delta f^{\rm ext}$ is the extrinsic increase in FWHM caused by defects and anisotropy dispersion in the Py films [27,28]. The red line represents the fitting curve using Eq. (5). The fitting brings about an $\alpha_{\rm eff}$ of 0.0120 ± 0.0014 for the Py metamolecule and of 0.0024 ± 0.0007 for the Py strip. $\Delta f^{\rm ext}$ of the Py metamolecule and strip are 0.3316 ± 0.0589 and 0.2192 ± 0.0155, respectively. $\alpha_{\rm eff}$ and $\Delta f^{\rm ext}$ increases in the metamolecule.

The parameters evaluated in the CPW-FMR measurements are summarized in Table I. Table I highlights that the Py metamolecule has smaller $g_{\rm eff}$ and $\mu_0 M_{\rm eff}$ and larger $\alpha_{\rm eff}$ and $\Delta f^{\rm ext}$ than those of the Py strip. The origin of a smaller $g_{\rm eff}$ is unclear. The smaller $\mu_0 M_{\rm eff}$ indicates surface and interface anisotropies due to unsaturated spins in the Py films on the SU8 film for the Py metamolecule. These unsaturated spins at the Py surface may reduce $g_{\rm eff}$ as pointed out by Shaw and co-workers [29]. The difference in $g_{\rm eff}$ between the Py metamolecule and Py strip might be due to the limited frequency and field range in the CPW-FMR measurements. Therefore, the data acquisition in a wider measurement range results in more accurate $g_{\rm eff}$ as well as $\mu_0 M_{\rm eff}$.

TABLE I. Parameters evaluated from fitting in Figs. 6(a) and 6(b) using Eqs. (3), (4), and (5).

	Py metamolecule	Py strip
$g_{\rm eff}$	2.1590 ± 0.0082	2.2800
$\mu_0 M_{\rm eff}$	681.77 ± 9.01	910.45
$\alpha_{\rm eff}$	0.0120 ± 0.0014	0.0024 ± 0.0007
$\Delta f^{\rm ext}$	0.3316 ± 0.0589	0.2192 ± 0.0155

Another possible origin for a decrease in $g_{\rm eff}$ is inhomogeneous ac magnetic fields generated by the microwaves, but this possibility is excluded by the following reasons. The ac-magnetic-field profiles around the CPW signal line are calculated. The calculation indicates that the ac-magnetic-field strengths perpendicular ($H_{\rm ac}^z$) and parallel ($H_{\rm ac}^x$) to the signal line are inhomogeneous. However, $H_{\rm ac}^z$, which is parallel to the dc magnetic field, does not contribute to FMR. Therefore, the inhomogeneous $H_{\rm ac}^z$ does not influence the FMR excitation (e.g., FMR frequency f_0). Additionally, the inhomogeneity in $H_{\rm ac}^x$ does not give any changes on f_0, since $H_{\rm ac}^x$ strength is sufficiently small (less than 0.05 mT) to allow the linear approximation of the Landau-Lifshitz-Gilbert equation. Hence, inhomogeneous ac magnetic fields are unlikely to be the origins for a decrease in $g_{\rm eff}$. While the inhomogeneous ac field does not influence $g_{\rm eff}$, it may affect the FWHM Δf in the FMR spectra, for example, by two-magnon scattering due to magnetization inhomogeneities [27,28]. Moreover, anisotropy dispersions, for example, magnetostriction anisotropy [30,31] and magnetic surface or interface anisotropy [29], induced by the coiling as well as the strain, mechanical cracks, and defects in the films give rise to magnetization inhomogeneities, resulting in an increase in $\Delta f^{\rm ext}$.

B. Magnetization configuration in the metamolecule

We observe the Kittel-mode FMR in the metamolecule by CPW FMR and cavity FMR at $\theta_H = 0°$. In the following, angle-resolved cavity FMR with varying θ_H reveals the magnetization configuration in the metamolecule. The cavity-FMR signals experimentally obtained in Fig. 3 are redrawn two-dimensionally (2D) in Fig. 7. White and blue correspond to high and low intensities in the derivative FMR signals, respectively. When $\theta_H = 0°$ and 180°, the magnetic field is applied uniformly to all portions in the Py MCh metamolecule, as illustrated in the lower inset in Fig. 7. The magnetization curves in Fig. 2 indicate that the Py metamolecule magnetization is easily saturated in this configuration. In this way, the Py metamolecule becomes a magnetic single-domain structure, resulting in a single resonance of the Kittel mode at around 106 mT excited at $\theta_H = 0°$ and 180°.

When the magnetic-field direction is oblique to the chiral axis ($0° < \theta_H < 180°$), the 2D plotted experimental results highlight two types resonances: One is shifted slightly to a lower field but excited around 100 mT at any angle, and the other is shifted significantly to a higher field as the angle θ_H is increased. For example, resonances at 117 and 134 mT when $\theta_H = 15°$ shift to much higher fields, as the θ_H is close to 90°. Since the Py metamolecule is the 3D structure, how the magnetic field is applied to the Py film is different in each portion of the metamolecule. When θ_H is 15°, the

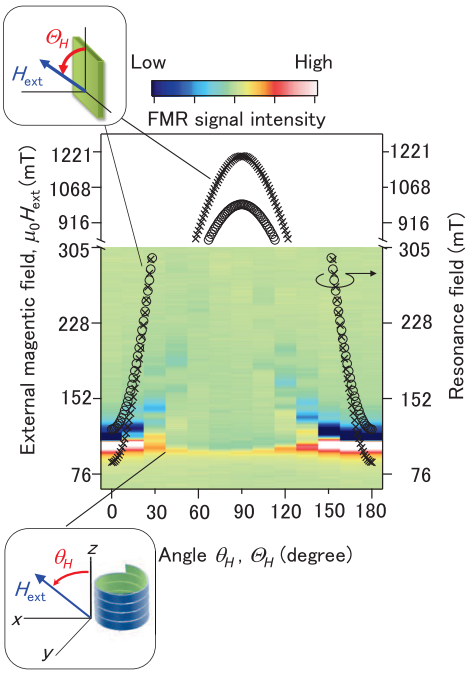

FIG. 7. The two-dimensional plot shows the FMR signal intensity of a single Py metamolecule obtained in Fig. 3 as a function of the angle (θ_H and Θ_H) and external dc magnetic field ($\mu_0 H_{ext}$). Angle θ_H (Θ_H) is defined in the lower (upper) inset. Open circles and crosses correspond to resonance fields calculated by the Kittel formula with the plane Py thin film model.

metamolecule's two aspects, which are parallel to the $x-z$ plane, are parallel to the magnetic field (see the inset in Fig. 7). In these two aspects, the magnetization direction follows the magnetic-field direction and the magnetization is easily saturated. The Kittel-mode resonance is thus observed around 100 mT at any angle. Contrastingly, magnetization in other portions, which are parallel to the y-z plane, is not parallel to the magnetic field (see the inset in Fig. 7). Kittel-mode FMR in these portions is an origin of the resonance significantly shifted to a higher field with an increase in θ_H.

The Kittel-mode resonance fields in a thin film calculated using Eq. (2) are plotted as a function of Θ_H in Fig. 7 (open circles). In the calculation, we use a $g_{\rm eff}$ of 2.16 and a $\mu_0 M_{\rm eff}$ of 681 mT evaluated from the Py metamolecule CPW-FMR results. At $\Theta_H = 0°$ the calculated resonance field is 121 mT. As Θ_H increases, the resonance shifts to a higher field owing to an increase in the demagnetization field. After reaching the maximum field of approximately 994 mT at $\Theta_H = 90°$, the resonance shifts to a lower field. Crosses correspond to the calculated resonance fields of the Kittel mode in a thin film, but $g_{\rm eff}$ and $\mu_0 M_{\rm eff}$ are the values experimentally evaluated from the Py strip CPW-FMR results. At $\Theta_H = 0°$ the calculated resonance field is 88 mT, which is smaller than the experimental value (106 mT) and previously calculated value (121 mT). At $\Theta_H = 90°$ the calculated resonance field is 1203 mT, which is higher than the calculated field using the metamolecules' $g_{\rm eff}$ and $\mu_0 M_{\rm eff}$.

The resonance fields shifting to a higher field with an increase in θ_H in the experiment are reproduced qualitatively by the calculation of the Kittel-mode FMR for a plane film with an in-plane magnetic field. This suggests that the magnetization configuration at $\theta_H = 0°$ and 180° is most likely to be the hollow-bar type. On the other hand, the magnetization configuration at remanent without external magnetic fields is likely to be azimuthal or helical, just similar to the corkscrew-type configuration [17], because the Py film is easily magnetized in the longitudinal direction of the strip. Indeed, rolled-up soft-magnetic microtubes of Py [32,33] and nickel [34] show azimuthally or helically magnetized domain structures at remanent.

Whereas the resonance-field shift is reproduced qualitatively by the calculation, the shift amount in experiments is much smaller than those calculated using Eq. (2). The difference between the calculation and experiment is owing to the calculation model. In the calculation, we assume a Py thin film with $g_{\rm eff}$ and $\mu_0 M_{\rm eff}$ evaluated from the CPW-FMR measurements. However, the Py metamolecule consists of the Py facets, which are parallel to the x-z plane or y-z plane, and the facets are connected to each other. The connecting curved regions between the facets is likely to be the origin of the contradiction.

The inhomogeneous magnetization in the connecting curved regions is indicated by the shifting Kittel-mode resonance signal in the angle-resolved cavity FMR. Figure 7 demonstrates that the shifting resonance by an oblique magnetic-field direction is accompanied by additional weak resonances at higher fields. In the aspects parallel to the y-z plane connected to curved regions, the magnetization is not saturated. Ring [35] and tubular [36] structures of a magnetic thin film in the unsaturated region exhibit the inhomogeneous magnetization configuration named the onionlike state. The onionlike state shows multiple resonance signals due to the localized resonance modes. Multiple resonance signals accompanied with the Kittel-mode FMR observed in the metamolecule are thus traced back to the localized resonance modes due to the inhomogeneous magnetization configuration, which is also indicated in the CPW-FMR results.

The resonance, which is almost independent of θ_H, shifts very slightly to a lower field as θ_H approaches 90°. The tiny shift of the resonance can be explained by the shape anisotropy of the Py strip in the metamolecules. The Py strip is magnetized in the direction of the strip width of 9 μm when $\theta_H = 0°$. On the other hand, when $\theta_H = 90°$, the Py film is easily magnetized in the direction of the strip length that is much larger than the width, bringing about a very small shift of the Kittel-mode resonance at 106 mT to a lower field of 97 mT. Such a small shift can be revealed in the present study, because the residual Py films are absent

on the substrate and the resonance signal is caused by only the single Py metamolecule.

IV. CONCLUSIONS

In this work, we investigate the FMR of a single MCh metamolecule of metallic Py at room temperature. The Py MCh metamolecule sample without residual Py films is prepared using the strain-driven self-coiling technique. Magnetization curves of ten metamolecules are obtained using AGM, and the saturation magnetization is 850 mT. A single metamolecule is picked up from the ten metamolecules and studied by angle-resolved FMR using a cavity. The cavity-FMR signal highlights two types of Kittel-mode FMR: One shifts slightly around 100 mT, and the other weak resonances shift significantly to a higher field as the magnetic field is applied perpendicular to the chiral axis. The shifting Kittel mode is accompanied by the multiple resonance signals caused by localized resonances with inhomogeneous magnetization, which is similar to the so-called onionlike state. The broadband CPW-FMR results fitted by the Kittel formula indicate a decrease in g_{eff} and $\mu_0 M_{\mathrm{eff}}$ and an increase in α_{eff} and Δf^{ext} for the Py metamolecule. The decrease in g_{eff} and $\mu_0 M_{\mathrm{eff}}$ is traced back to magnetic surface or interface anisotropy, whereas the increase in Δf^{ext} is caused by an inhomogeneous ac magnetic field and magnetization inhomogeneities due to anisotropy dispersions, e.g., strain-induced magnetostriction anisotropy and magnetic surface or interface anisotropy, in the Py metamolecule.

We reveal in this study that, when the magnetic field is parallel to the chiral axis, the magnetization in the metamolecule is aligned to the magnetic-field direction; the magnetization configuration of the Py MCh metamolecule is the hollow-bar type, although the magnetization configuration at remanent is likely to be the corkscrew type. The hollow-bar-type magnetization configuration is essential for obtaining the directional birefringence independent of polarization. The present study opens the door to the realization of MCh metamaterials as artificial gauge fields for manipulating electromagnetic waves in the millimeter wave and terahertz wave regions, bringing about nonreciprocal optical elements like a direction-switchable "one-way mirror" using magnetic fields. Additionally, the MCh metamolecules, in which time-reversal and space-inversion symmetries are broken simultaneously, enable us to mimic natural multiferroic materials at a modest magnetic field and room temperature. When we succeed in preparing nanometer-scaled metamolecules, it will also be interesting to compare chiral domains predicted in magnetic nanotube structures [37].

ACKNOWLEDGMENTS

The authors are grateful to A. Yoshida and Y. Kusanagi for technical assistance and to L. McDowell for English proofreading. T. Kodama acknowledges a Grant-in-Aid for JSPS Fellows. S. T. acknowledges the partial support of this work by JSPS KAKENHI (No. 26287065). A part of this work was conducted at the Nagoya University Nanofabrication Platform supported by "Nanotechnology Platform Program" and at Tohoku University under the Cooperative Research Program of "Network Joint Research Center for Materials and Devices" of MEXT, Japan.

[1] E. Hecht, *Optics* (Pearson Education, Boston, Massachusetts, 2013).
[2] L. D. Barron and J. Vrbancich, Magneto-chiral birefringence and dichroism, Mol. Phys. **51**, 715 (1984).
[3] G. L. J. A. Rikken and E. Raupach, Observation of magneto-chiral dichroism, Nature (London) **390**, 493 (1997).
[4] P. Kleindienst and G. H. Wagnière, Interferometric detection of magnetochiral birefringence, Chem. Phys. Lett. **288**, 89 (1998).
[5] M. Vallet, R. Ghosh, A. Le Floch, T. Ruchon, F. Bretenaker, and J.-Y. Thépot, Observation of Magnetochiral Birefringence, Phys. Rev. Lett. **87**, 183003 (2001).
[6] C. Train, R. Gheorghe, V. Krstic, L.-M. Chamoreau, N. S. Ovanesyan, G. L. J. A. Rikken, M. Gruselle, and M. Verdaguer, Strong magneto-chiral dichroism in enantiopure chiral ferromagnets, Nat. Mater. **7**, 729 (2008).
[7] I. Kézsmárki, D. Szaller, S. Bordàcs, V. Kocsis, Y. Tokunaga, Y. Taguchi, H. Murakawa, Y. Tokura, H. Engelkamp, T. Rõõm, and U. Nagel, One-way transparency of four-coloured spin-wave excitations in multiferroic materials, Nat. Commun. **5**, 3203 (2014).
[8] K. Sawada and N. Nagaosa, Optical Magnetoelectric Effect in Multiferroic Materials: Evidence for a Lorentz Force Acting on a Ray of Light, Phys. Rev. Lett. **95**, 237402 (2005).
[9] K. Fang, Z. Yu, and S. Fan, Realizing effective magnetic field for photons by controlling the phase of dynamic modulation, Nat. Photonics **6**, 782 (2012).
[10] S. Mühlbauer, B. Binz, F. Jonietz, C. Pfleiderer, A. Rosch, A. Neubauer, R. Georgii, and P. Böni, Skyrmion lattice in a chiral magnet, Science **323**, 915 (2009).
[11] S. Bordàcs, I. Kézsmárki, D. Szaller, L. Demkó, N. Kida, H. Murakawa, Y. Onose, R. Shimano, T. Rõõm, U. Nagel, S. Miyahara, N. Furukawa, and Y. Tokura, Chirality of matter shows up via spin excitations, Nat. Phys. **8**, 734 (2012).
[12] D. R. Smith, Willie J. Padilla, D. C. Vier, S. C. Nemat-Nasser, and S. Schultz, Composite Medium with Simultaneously Negative Permeability and Permittivity, Phys. Rev. Lett. **84**, 4184 (2000).
[13] S. Tomita, K. Sawada, A. Porokhnyuk, and T. Ueda, Direct Observation of Magnetochiral Effects through a Single Metamolecule in Microwave Regions, Phys. Rev. Lett. **113**, 235501 (2014).
[14] M. Huang, F. Cavallo, F. Liu, and M. G. Lagally, Nanomechanical architecture of semiconductor nanomembranes, Nanoscale **3**, 96 (2011).
[15] F. Balhorn, S. Mansfeld, A. Krohn, J. Topp, W. Hansen, D. Heitmann, and S. Mendach, Spin-Wave Interference in Three-Dimensional Rolled-Up Ferromagnetic Microtubes, Phys. Rev. Lett. **104**, 037205 (2010).

[16] E. J. Smith, Z. Liu, Y. Mei, and O. G. Schmidt, Combined surface plasmon and classical waveguiding through metamaterial fiber design, Nano Lett. **10**, 1 (2010).

[17] E. J. Smith, D. Makarov, S. Sanchez, V. M. Fomin, and O. G. Schmidt, Magnetic Microhelix Coil Structures, Phys. Rev. Lett. **107**, 097204 (2011).

[18] C. Müller, C. C. Bof Bufon, M. E. Navarro Fuentes, D. Makarov, D. H. Mosca, and O. G. Schmidt, Towards compact three-dimensional magnetoelectronics-magnetoresistance in rolled-up Co/Cu nanomembranes, Appl. Phys. Lett. **100**, 022409 (2012).

[19] Ch. Strelow, C. M. Schultz, H. Rehberg, M. Sauer, H. Welsch, A. Stemmann, Ch. Heyn, D. Heitmann, and T. Kipp, Light confinement and mode splitting in rolled-up semiconductor microtube bottle resonators, Phys. Rev. B **85**, 155329 (2012).

[20] C.-C. Chen, A. Ishikawa, Y.-H. Tang, M.-H. Shiao, D. P. Tsai, and T. Tanaka, Uniaxial-isotropic metamaterials by three-dimensional split-ring resonators, Adv. Opt. Mater. **3**, 44 (2015).

[21] T. Kodama, S. Tomita, N. Hosoito, and H. Yanagi, Fabrication and ferromagnetic resonance of cobalt chiral meta-molecule arrays, Appl. Phys. A **122**, 41 (2016).

[22] E. J. Smith, D. Makarov, and O. G. Schmidt, Polymer delamination: Towards unique three-dimensional microstructures, Soft Matter **7**, 11309 (2011).

[23] J. P. Nibarger, R. Lopusnik, Z. Celinski, and T. J. Silva, Variation of magnetization and the Landé g factor with thickness in Ni-Fe films, Appl. Phys. Lett. **83**, 93 (2003).

[24] C. Kittel, *Introduction to Solid State Physics*, 7th ed. (Wiley, New York, 1995).

[25] Y. Ajiro, H. Yazawa, K. Kawaguchi, N. Hosoito, and T. Shinjo, Ferromagnetic resonance of Fe/Mg multilayer films with artificial superstructure, J. Phys. Soc. Jpn. **58**, 3339 (1989).

[26] J. M. Shaw, H. T. Nembach, and T. J. Silva, Determination of spin pumping as a source of linewidth in sputtered $Co_{90}Fe_{10}$/Pd multilayers by use of broadband ferromagnetic resonance spectroscopy, Phys. Rev. B **85**, 054412 (2012).

[27] C. E. Patton, C. H. Wilts, and F. B. Humphrey, Relaxation processes for ferromagnetic resonance in thin films, J. Appl. Phys. **38**, 1358 (1967).

[28] B. Heinrich, J. F. Cochran, and R. Hasegawa, FMR linebroadening in metals due to two-magnon scattering, J. Appl. Phys. **57**, 3690 (1985).

[29] J. M. Shaw, H. T. Nembach, T. J. Silva, and C. T. Boone, Precise determination of the spectroscopic g-factor by use of broadband ferromagnetic resonance spectroscopy, J. Appl. Phys. **114**, 243906 (2013).

[30] C.-Y. Hung, M. Mao, S. Funada, T. Schneider, L. Miloslavsky, M. Miller, C. Qian, and H. C. Tong, Magnetic properties of ultrathin NiFe and CoFe films, J. Appl. Phys. **87**, 6618 (2000).

[31] N. Pérez, M. Melzer, D. Makarov, O. Ueberschär, R. Ecke, S. E. Schulz, and O. G. Schmidt, High-performance giant magnetoresistive sensorics on flexible Si membranes, Appl. Phys. Lett. **106**, 153501 (2015).

[32] R. Streubel, J. Lee, D. Makarov, Mi-Young Im, D. Karnaushenko, L. Han, R. Schäfer, P. Fischer, Sang-Koog Kim, and O. G. Schmidt, Magnetic microstructure of rolled-up single-layer ferromagnetic nanomembranes, Adv. Mater. **26**, 316 (2014).

[33] R. Streubel, L. Han, F. Kronast, A. A. Ünal, O. G. Schmidt, and D. Makarov, Imaging of buried 3D magnetic rolled-up nanomembranes, Nano Lett. **14**, 3981 (2014).

[34] R. Streubel, F. Kronast, P. Fischer, D. Parkinson, O. G. Schmidt, and D. Makarov, Retrieving spin textures on curved magnetic thin films with full-field soft X-ray microscopies, Nat. Commun. **6**, 7612 (2015).

[35] F. Giesen, J. Podbielski, and D. Grundler, Mode localization transition in ferromagnetic microscopic rings, Phys. Rev. B **76**, 014431 (2007).

[36] S. Mendach, J. Podbielski, J. Topp, W. Hansen, and D. Heitmann, Spin-wave confinement in rolled-up ferromagnetic tubes, Appl. Phys. Lett. **93**, 262501 (2008).

[37] P. Landeros and Álvaro S. Núñez, Domain wall motion on magnetic nanotubes, J. Appl. Phys. **108**, 033917 (2010).